Low-Dispersion Wake Field Calculation Tools*

Mikko Kärkkäinen†, Erion Gjonaj‡, Thomas Lau§, Thomas Weiland¶
Technische Universitaet Darmstadt, Institut fuer Theorie Electromagnetischer Felder (TEMF)
Schlossgartenstrasse 8, 64289 Darmstadt, Germany

Abstract

Wide-band finite-difference time-domain (FDTD) algorithms for wake field simulations in accelerator structures are presented. The schemes are based on enlarged stencils enabling explicit updating of the variables over time. An elaborated dispersion analysis verifies that the schemes propagate plane waves in major coordinate axis directions without numerical dispersion. The methods are validated by comparing numerical results with results obtained by other methods. The important issue of calculating wake potentials in general 3D structures is addressed.

INTRODUCTION

Very short bunches (rms length in the sub-millimeter range) will be used in future linear colliders. To be able to propagate these short bunches numerically through a long structure (several kilometers), billions of mesh cells are needed in the longitudinal direction. To avoid accumulation of dispersion errors during the numerical simulation, a numerical scheme should ideally be free of numerical dispersion at least in the longitudinal direction. Several methods with this feature have been published [1, 2, 3, 4, 5]. In large problems, the simulation time becomes very long, and it is desirable to parallelize the codes. Explicit schemes are usually computationally more effective and easier to parallelize than implicit schemes.

THE PROBLEM FORMULATION

The beam is assumed to propagate rigidly, i.e., the wake fields generated by the bunch do not affect the particle distribution within the bunch. The beam is also assumed to propagate with the velocity of light along the z-axis. An ultra-relativistic bunch ($v = c$) with a linear charge distribution

$$\rho(x, y, z, t) = \delta(x)\delta(y)\lambda(z - ct) \tag{1}$$

in free space creates a radial electric field distribution of the form

$$E_r(x, y, z, t) = \frac{\rho(x, y, z, t)}{2\pi\epsilon_0\sqrt{x^2 + y^2}}. \tag{2}$$

The field dynamics is governed by the Maxwell's equations:

$$\nabla \times \mathbf{H} = \frac{\partial \mathbf{D}}{\partial t} + \mathbf{J}, \quad \nabla \times \mathbf{E} = -\frac{\partial \mathbf{B}}{\partial t}, \qquad \nabla \cdot \mathbf{D} = \rho, \quad \nabla \cdot \mathbf{B} = 0. \tag{3}$$

The scattered field formalism is used in this paper. Hence, the excitation is embedded in boundary conditions and the current density $\mathbf{J}$ vanishes inside the computational domain. Cylindrically symmetric problems are dealt with using a scalar potential as described in the next section.

THE NUMERICAL SCHEMES

Finite-difference schemes are usually based on solving the Maxwell's curl equations (4) iteratively in time and space. The divergence equations are not explicitly enforced in FDTD/FIT schemes [6, 7]. While the numerical divergence vanishes for some schemes [6, 7], it is non-zero for others [3]. A general operator splitting method is discussed in [8], and has been applied to derive specific schemes in [3]. We will focus on the curl equations in 3D and use a scalar potential in 2D problems.

3D Scheme

Consider updating the x-component of the electric field. The basic idea of the scheme is to enlarge the stencil allowing a larger time step than with the Yee scheme. The finite-difference operators presented for narrow-band applications in [9, 10] are modified and used here for wide-band calculations. Thus, the operators are used without assumptions on the frequency. The update equation for E_x in free space reads:

$$\begin{aligned} E_x|^{n+1}_{i+1/2,j,k} = E_x|^{n}_{i+1/2,j,k} \quad & - \\ \alpha\frac{\Delta t}{\epsilon_0} D_{z,0} H_y|^{n+1/2}_{i+1/2,j,k} \quad & - \\ 4\beta\frac{\Delta t}{\epsilon_0} D_{z,1} H_y|_{i+1/2,j,k} \quad & - \\ 4\gamma\frac{\Delta t}{\epsilon_0} D_{z,2} H_y|^{n+1/2}_{i+1/2,j,k} \quad & + \\ \alpha\frac{\Delta t}{\epsilon_0} D_{y,0} H_z|^{n+1/2}_{i+1/2,j,k} \quad & + \\ 4\beta\frac{\Delta t}{\epsilon_0} D_{y,1} H_z|^{n+1/2}_{i+1/2,j,k} \quad & + \\ 4\gamma\frac{\Delta t}{\epsilon_0} D_{y,2} H_z|^{n+1/2}_{i+1/2,j,k}. & \end{aligned} \tag{4}$$

Here the three spatial derivative operators are all second-order accurate by construction (center differences). The

* Work supported by EUROTeV (RIDS-011899), EUROFEL (RIDS-011935), DFG (1239/22-3) and DESY Hamburg
† mikko@temf.tu-darmstadt.de
‡ gjonaj@temf.tu-darmstadt.de
§ lau@temf.tu-darmstadt.de
¶ thomas.weiland@temf.tu-darmstadt.de

operator $D_{z,0}$ is the familiar center difference operator as used in the standard Yee FDTD [6] scheme. The other two operators $D_{z,1}$ and $D_{z,2}$ are weighted averages of similar center differences defined at different positions in space. The averages are taken symmetrically in space to guarantee second-order accuracy. The spatial derivatives in (4) are defined by

$$\begin{aligned}
D_{z,0}H_y|^{n+1/2}_{i+1/2,j,k} &= \\
&\frac{H_y|^{n+1/2}_{i+1/2,j,k+1/2} - H_y|^{n+1/2}_{i+1/2,j,k-1/2}}{\Delta z}, \\
D_{z,1}H_y|^{n+1/2}_{i+1/2,j,k} &= \\
&\frac{H_y|^{n+1/2}_{i+1/2,j+1,k+1/2} - H_y|^{n+1/2}_{i+1/2,j+1,k-1/2}}{4\Delta z} + \\
&\frac{H_y|^{n+1/2}_{i+1/2,j-1,k+1/2} - H_y|^{n+1/2}_{i+1/2,j-1,k-1/2}}{4\Delta z} + \\
&\frac{H_y|^{n+1/2}_{i+3/2,j,k+1/2} - H_y|^{n+1/2}_{i+3/2,j,k-1/2}}{4\Delta z} + \\
&\frac{H_y|^{n+1/2}_{i-1/2,j,k+1/2} - H_y|^{n+1/2}_{i-1/2,j,k-1/2}}{4\Delta z}, \\
D_{z,2}H_y|^{n+1/2}_{i+1/2,j,k} &= \\
&\frac{H_y|^{n+1/2}_{i+3/2,j+1,k+1/2} - H_y|^{n+1/2}_{i+3/2,j+1,k-1/2}}{4\Delta z} + \\
&\frac{H_y|^{n+1/2}_{i-1/2,j-1,k+1/2} - H_y|^{n+1/2}_{i-1/2,j-1,k-1/2}}{4\Delta z} + \\
&\frac{H_y|^{n+1/2}_{i+3/2,j-1,k+1/2} - H_y|^{n+1/2}_{i+3/2,j-1,k-1/2}}{4\Delta z} + \\
&\frac{H_y|^{n+1/2}_{i-1/2,j+1,k+1/2} - H_y|^{n+1/2}_{i-1/2,j+1,k-1/2}}{4\Delta z}.
\end{aligned} \tag{5}$$

The update equations for the E_y and E_z are obtained by permuting the indices. The calculation of the z-derivative of the magnetic field is illustrated in Fig. 1.

As we are using the scattered field formalism, the boundary conditions for the tangential electric fields on the PEC (Perfect Electric Conductor) boundaries are given by

$$E_t^{scat} = -E_t^{inc} \tag{6}$$

since the total tangential electric field $E_t^{tot} = E_t^{scat} + E_t^{inc} = 0$ on PEC interfaces. The components of E_t^{inc} can be evaluated from (2) in the computer code.

The magnetic field update equations are the same as with the Yee scheme, i.e.

$$\begin{aligned}
H_x|^{n+1/2}_{i,j+1/2,k+1/2} &= H_x|^{n-1/2}_{i,j+1/2,k+1/2} - \\
&\frac{\Delta t}{\mu_0 \Delta y}(E_z|^n_{i,j+1,k+1/2} - E_z|^n_{i,j,k+1/2}) + \\
&\frac{\Delta t}{\mu_0 \Delta z}(E_y|^n_{i,j+1/2,k+1} - E_y|^n_{i,j+1/2,k})
\end{aligned} \tag{7}$$

and analogously for the H_y and H_z. The standard FDTD update equations as proposed by Yee are obtained by letting $\alpha = 1$, $\beta = \gamma = 0$. However, as will be shown subsequently, the numerical waves propagate much more isotropically with another choice of parameters α, β and γ. With accelerator applications in mind, it is a significant feature of the proposed scheme that the dispersion properties can be improved while at the same time increasing the stable time step to the so-called magic time step $\Delta t = \Delta z/c$. This time step allows the use of a moving window [15] in long time simulations without numerical dispersion in the longitudinal direction.

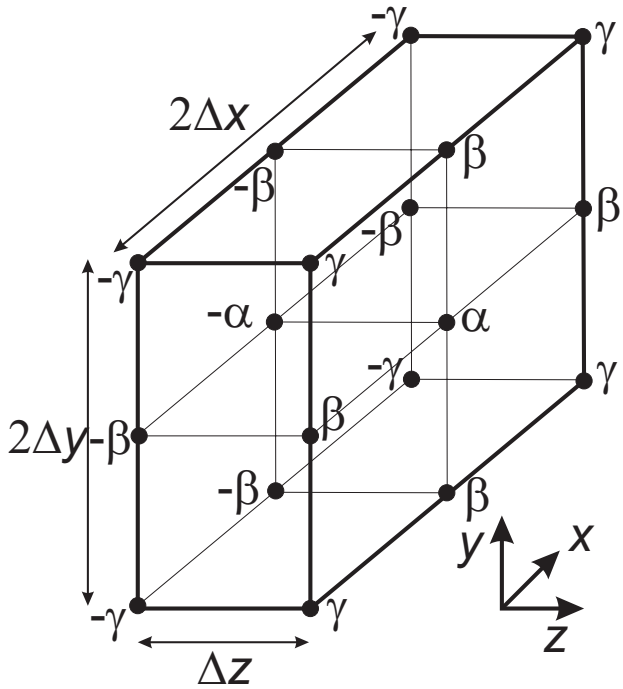

Figure 1: Graphical description to calculate the z-derivative of the magnetic field located in the center of the box. The indicated weights are assigned to the magnetic field values at the corresponding vertices.

2D Scheme Based on a Potential Formalism

Here we will introduce a new explicit scheme that can be used in the special case of cylindrically symmetric structures. Starting from the Maxwell's equations in cylindrical coordinates

$$\begin{aligned}
\epsilon_z \frac{\partial E_z}{\partial t} &= \frac{1}{r}\frac{\partial (rH_\phi)}{\partial r}, \\
\epsilon_r \frac{\partial E_r}{\partial t} &= -\frac{\partial H_\phi}{\partial z}, \\
\mu_\phi \frac{\partial H_\phi}{\partial t} &= \frac{\partial E_z}{\partial r} - \frac{\partial E_r}{\partial z}.
\end{aligned} \tag{8}$$

we define a scalar potential Φ as

$$\Phi(r,z,t) = \int_0^r r' E_z^{scat}(r',z,t)\, dr' \tag{9}$$

and obtain the following second-order partial differential equation (PDE) for the potential:

$$\frac{\partial^2\Phi}{c^2\partial t^2} = \frac{\partial^2\Phi}{\partial z^2} + \frac{\partial^2\Phi}{\partial r^2} - \frac{1}{r}\frac{\partial\Phi}{\partial r}. \tag{10}$$

This has been solved in [4] and [5] *implicitly* such that there is no numerical dispersion in z-direction. We will solve the equation *explicitly* so that there is no dispersion in $z-$ and r-directions.

The PDE can be discretized using the standard second-order center differences for the time-derivatives and spatial averaging of center differences for the spatial derivatives. As an example, consider the discrete version of the second-order z-derivative at the spatial position $(z, r) = (i\Delta z, m\Delta r)$ and at time moment $t = n\Delta t$:

$$\begin{aligned}\frac{\partial^2\Phi}{\partial z^2}|^n_{i,m} &= b_z\frac{\Phi|^n_{i+1,m-1} - 2\Phi|^n_{i,m-1} + \Phi|^n_{i-1,m-1}}{\Delta z^2} \\ &+ a_z\frac{\Phi|^n_{i+1,m} - 2\Phi|^n_{i,m} + \Phi|^n_{i-1,m}}{\Delta z^2} \\ &+ b_z\frac{\Phi|^n_{i+1,m+1} - 2\Phi|^n_{i,m+1} + \Phi|^n_{i-1,m+1}}{\Delta z^2}\end{aligned} \tag{11}$$

where $a_z + 2b_z = 1$. The second-order r-derivative is discretized similarly. However, the first-order term is calculated as

$$\begin{aligned}\frac{1}{r}\frac{\partial\Phi}{\partial r}|^n_{i,m} &= \frac{1}{m\Delta r}\left[\frac{\Phi|^n_{i-1,m+1} - \Phi|^n_{i-1,m-1}}{4\Delta r}\right. \\ &+ \frac{\Phi|^n_{i,m+1} - \Phi|^n_{i,m-1}}{2\Delta r} \\ &+ \left.\frac{\Phi|^n_{i+1,m+1} - \Phi|^n_{i+1,m-1}}{4\Delta r}\right]\end{aligned} \tag{12}$$

regardless of the parameters a_z and a_r. Notice that the singularity at $m = 0$ does not pose a problem since it occurs on the axis where we explicitly set $\Phi = 0$ due to cylindrical symmetry. For a general cell aspect ratio $\rho = \Delta r/\Delta z \geq 1$ we use

$$a_z = a_r = \frac{1 + 2\rho^2}{2 + 2\rho^2}, \quad b_z = b_r = \frac{1}{4(1 + \rho^2)}. \tag{13}$$

Using the second equation of (8) and the definition of the potential (9) it is easy to show that the boundary condition on boundaries $z = const$ takes the form

$$\frac{\partial\Phi}{\partial z} = -rE^{scat}_r = rE^{inc}_r \tag{14}$$

because $E^{tot}_r = E^{scat}_r + E^{inc}_r = 0$ on the PEC boundary. Notice that the incident field E^{inc}_r can be imposed using the analytical field distribution of an ultrarelativistic bunch (2) where λ is a linear charge distribution. A typically used gaussian charge distribution is given by

$$\lambda(s) = \frac{q}{\sqrt{2\pi}\sigma}e^{-\frac{s^2}{2\sigma^2}} \tag{15}$$

where σ is the rms length of the bunch.

On boundaries $r = const$ we obtain from (9) the boundary condition

$$\frac{\partial\Phi}{\partial r} = rE^{scat}_z = -rE^{inc}_z = 0 \tag{16}$$

because there is no longitudinal component of the incident field. With a staircased geometry approximation, the boundary conditions are based on these expressions (14)-(16).

NUMERICAL DISPERSION

In this section we compare the numerical dispersion of the proposed 3D and 2D schemes with others.

3D Scheme

The dispersion properties of the scheme can be found by performing the von Neumann dispersion analysis. A plane electromagnetic wave

$$\begin{aligned}\mathbf{E} &= \mathbf{E}_0 e^{j(k_x x + k_y y + k_z z - \omega t)}, \\ \mathbf{H} &= \mathbf{H}_0 e^{j(k_x x + k_y y + k_z z - \omega t)}.\end{aligned} \tag{17}$$

is inserted into the discrete equations. The dispersion relation follows by requiring nontrivial solutions to the homogeneous linear system:

$$\mathbf{det}(A) = 0 \tag{18}$$

where the matrix elements $a_{i,j}, i, j = 1, 2, 3$ are defined as

$$\begin{aligned}
a_{1,1} &= \sin^2(\frac{\omega\Delta t}{2}) - \frac{\Delta t}{\epsilon_x\Delta y}\sin(\frac{k_y y}{2})\frac{\Delta t}{\mu_z\Delta y}\sin(\frac{k_y y}{2})C_{x,z} \\
&- \frac{\Delta t}{\epsilon_x\Delta z}\sin(\frac{k_z z}{2})\frac{\Delta t}{\mu_y\Delta z}\sin(\frac{k_z z}{2})C_{x,y}, \\
a_{1,2} &= \frac{\Delta t}{\epsilon_x\Delta y}\sin(\frac{k_y y}{2})\frac{\Delta t}{\mu_z\Delta x}\sin(\frac{k_x x}{2})C_{x,z}, \\
a_{1,3} &= \frac{\Delta t}{\epsilon_x\Delta z}\sin(\frac{k_z z}{2})\frac{\Delta t}{\mu_y\Delta x}\sin(\frac{k_x x}{2})C_{x,y}, \\
a_{2,1} &= \frac{\Delta t}{\epsilon_y\Delta x}\sin(\frac{k_x x}{2})\frac{\Delta t}{\mu_z\Delta y}\sin(\frac{k_y y}{2})C_{y,z}, \\
a_{2,2} &= \sin^2(\frac{\omega\Delta t}{2}) - \frac{\Delta t}{\epsilon_y\Delta z}\sin(\frac{k_z z}{2})\frac{\Delta t}{\mu_x\Delta z}\sin(\frac{k_z z}{2})C_{x,y} \\
&- \frac{\Delta t}{\epsilon_y\Delta x}\sin(\frac{k_x x}{2})\frac{\Delta t}{\mu_z\Delta x}\sin(\frac{k_x x}{2})C_{y,z}, \\
a_{2,3} &= \frac{\Delta t}{\epsilon_y\Delta z}\sin(\frac{k_z z}{2})\frac{\Delta t}{\mu_x\Delta y}\sin(\frac{k_y y}{2})C_{x,y}, \\
a_{3,1} &= \frac{\Delta t}{\epsilon_z\Delta x}\sin(\frac{k_x x}{2})\frac{\Delta t}{\mu_y\Delta z}\sin(\frac{k_z z}{2})C_{y,z}, \\
a_{3,2} &= \frac{\Delta t}{\epsilon_z\Delta y}\sin(\frac{k_y y}{2})\frac{\Delta t}{\mu_x\Delta z}\sin(\frac{k_z z}{2})C_{x,z}, \\
a_{3,3} &= \sin^2(\frac{\omega\Delta t}{2}) - \frac{\Delta t}{\epsilon_z\Delta x}\sin(\frac{k_x x}{2})\frac{\Delta t}{\mu_y\Delta x}\sin(\frac{k_x x}{2})C_{y,z} \\
&- \frac{\Delta t}{\epsilon_z\Delta y}\sin(\frac{k_y y}{2})\frac{\Delta t}{\mu_x\Delta y}\sin(\frac{k_y y}{2})C_{x,z}.
\end{aligned} \tag{19}$$

and the parameters $C_{x,y}$, $C_{x,z}$ and $C_{y,z}$ are given by

$$\begin{aligned} C_{x,y} &= \alpha + 2\beta(\cos(k_x\Delta x) + \cos(k_y\Delta y)) \\ &+ 4\gamma\cos(k_x x)\cos(k_y y), \\ C_{x,z} &= \alpha + 2\beta(\cos(k_x\Delta x) + \cos(k_z\Delta z)) \\ &+ 4\gamma\cos(k_x x)\cos(k_z z), \\ C_{y,z} &= \alpha + 2\beta(\cos(k_y\Delta y) + \cos(k_z\Delta z)) \\ &+ 4\gamma\cos(k_y y)\cos(k_z z). \end{aligned} \quad (20)$$

For cubic cells ($\Delta = \Delta x = \Delta y = \Delta z$) the scheme is stable with $\alpha = 7/12, \beta = 1/12$ and $\gamma = 1/48$ up to the time step $\Delta t = \Delta z/c$. These parameters are used in subsequent dispersion plots. In spherical coordinates, we can express the components of the wave vector $\mathbf{k} = k_x\mathbf{u}_x + k_y\mathbf{u}_y + k_z\mathbf{u}_z$ as

$$\begin{aligned} k_x &= k\cos(\phi)\sin(\theta) \\ k_y &= k\sin(\phi)\sin(\theta) \\ k_z &= k\cos(\theta) \end{aligned} \quad (21)$$

where $k = |\mathbf{k}|$ and ϕ is the azimuthal and θ is the elevation angle. The wave number k of the numerical scheme as a function of propagation direction can be solved numerically from equations (18)-(21). Let $N_\lambda = \lambda/\Delta$. We

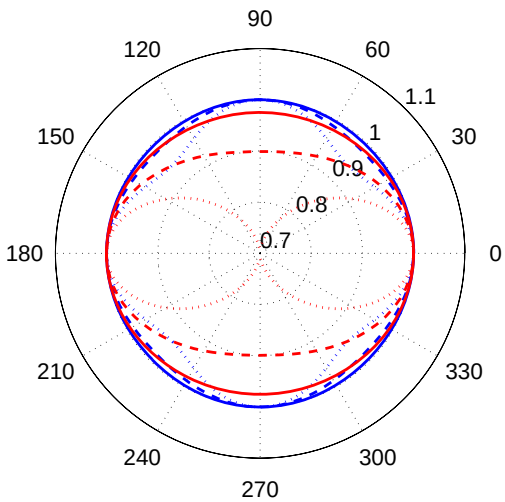

Figure 2: Normalized numerical phase velocity (v_p/c) as a function of θ in xz-plane. Blue curves: proposed scheme. Red curves: LT splitting [3]. Dotted lines: $N_\lambda = 3$. Dashed lines: $N_\lambda = 5$. Solid lines: $N_\lambda = 10$.

will compare the numerical dispersion properties of the proposed scheme and the LT splitting scheme [3] that is the basis of a recently developed computer code PBCI [11] (*Parallelized Beam Cavity Interaction*).

The numerical phase velocity normalized with the velocity of light on xz-plane is shown in Fig. 2. An identical plot is obtained on the yz-plane with both of the schemes. It is observed that the phase velocity error vanishes with the proposed scheme in $\pm x$ and $\pm z$ -directions regardless of spatial resolution. It is also seen that with the proposed scheme the anisotropy of the phase velocity is significantly lower than with the LT splitting scheme with a fixed spatial resolution $N_\lambda = \lambda/\Delta z$. The comparison in Fig. 3 with the standard Yee FDTD scheme [6] reveals that the phase velocity error is almost uniformly lower with the proposed scheme than with the Yee scheme. The special feature of zero dispersion in $\pm x$, $\pm y$ and $\pm z$ directions can be seen.

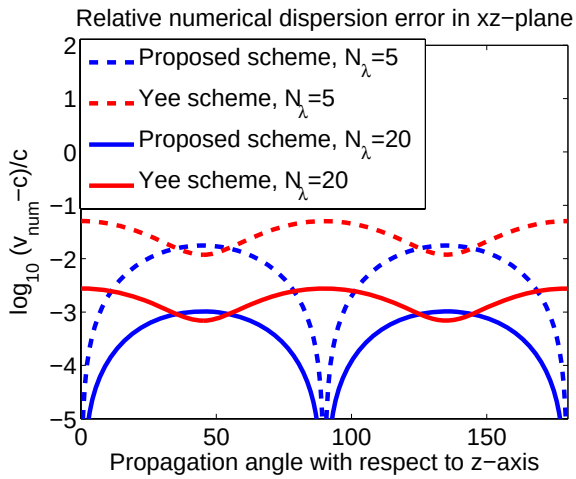

Figure 3: Relative error of the phase velocity in xz-plane with different mesh resolutions ($N_\lambda = \lambda/\Delta z$). Comparison of the proposed scheme with the Yee scheme.

2D Scheme

Now the numerical dispersion of the 2D scheme is analyzed. Let θ be the angle between $\mathbf{k}$ and the z-axis and $|\mathbf{k}| = k$. Consider a plane electromagnetic wave of the form

$$\Phi = \Phi_0 e^{-j(k\cos(\theta)x + k\sin(\theta)y - \omega t)}. \quad (22)$$

To derive the numerical dispersion equation, we use $t = n\Delta t$ and $z = i\Delta z$, $r = m\Delta r$ and insert this ansatz into (10), obtaining

$$\begin{aligned} 2\sin^2(\frac{\omega\Delta t}{2}) + (\frac{c_0\Delta t}{\Delta z})^2 \quad &\times \\ [\cos(k\Delta z\cos\theta) \quad &\times \\ (1 - 4b_z\sin^2(\frac{k\Delta r\sin\theta}{2}) - \frac{2b_r\Delta z^2}{\Delta r^2}) \quad &+ \\ \frac{\Delta z^2}{\Delta r^2}\cos(k\Delta r\sin\theta) \quad &\times \\ (1 - 4b_z\sin^2(\frac{k\Delta r\cos\theta}{2}) - \frac{2b_r\Delta r^2}{\Delta z^2}) \quad &- \\ a_z - \frac{\Delta z^2}{\Delta r^2}a_r \quad &- \\ \frac{j\Delta z^2}{4m\Delta r^2}\cos(\frac{k\Delta z\cos\theta}{2})^2\sin(k\Delta r\sin\theta)\Big] & \end{aligned} \quad (23)$$

Considering the special case $\theta = 0$ (i.e. propagation in z-direction) it is easy to show that the numerical phase velocity equals the velocity of light in vacuum. Let us take the

angle θ as a parameter and plot the numerical phase velocity as a function of θ for few mesh resolutions $N_\lambda = \lambda/\Delta z$ (here $\Delta z = \Delta r$ is assumed). In Fig. 4, numerical phase velocity is illustrated for the explicit and the implicit [5] schemes for various mesh resolutions. With the explicit scheme, the anisotropy of the phase velocity is very low if 20 cells over the bunch length are used. The scheme is free of numerical dispersion in longitudinal and in transversal directions for any (meaningful) spatial resolution.

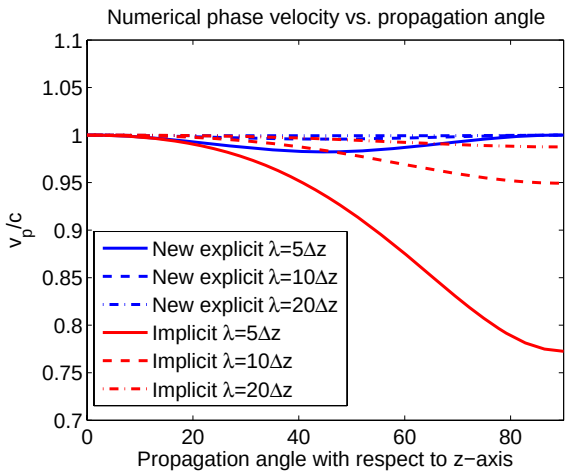

Figure 4: Numerical phase velocity with the new explicit scheme and with the implicit scheme of [5].

VALIDATION OF THE PROPOSED SCHEMES

Wake field codes for circular cylindrically symmetric structures have been successfully used for a long time [14, 4, 5]. Also, the indirect method for wake potential calculations has been implemented and verified for cylindrically symmetric problems [13, 5]. The recently published scheme for calculating wake potentials in arbitrary 3D structures [16] is adopted here. Another approach to perform the indirect integration in wake field calculations is presented in [17]. The schemes [16, 17] allow to truncate the outgoing beam pipe in the numerical code without the need to time-march through the long outgoing beam pipe. According to [16], on the plane *at the end of the truncated structure*, one has to solve a Poisson's equation at each time step in the end of the numerical simulation. We have implemented the scheme in [16] and compared with 2D reference results. The 2D results are obtained with the presented explicit low-dispersion variant of the schemes [4, 5]. As a test structure we have chosen the circular cylindrically symmetric step collimator in Fig. 5 (a). The longitudinal wake potentials as obtained with the proposed 3D scheme and with the 2D scheme are shown in Fig. 5 (b). The rms bunch length is $\sigma = 200\ \mu m$. The agreement is excellent. The proposed 3D scheme is also validated by simulating a practical ILC collimator structure and by comparing with results obtained with another

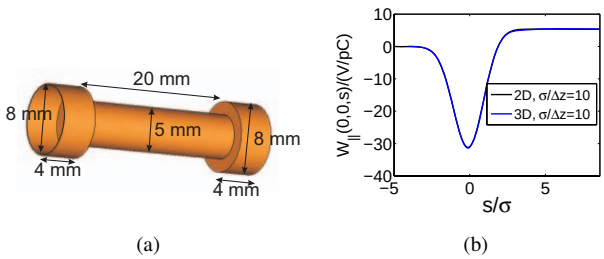

(a) (b)

Figure 5: (a) A cylindrically symmetric step collimator. (b) Longitudinal wake potentials.

3D scheme. The collimator was built for experimental tests carried out with SLAC, USA. The geometry of the collimator is shown in Fig. 6. For validation purposes, we choose a rms bunch length [1] of $\sigma = 1.0$ mm and compare with the parallelized computer code PBCI [11]. The proposed scheme has not been parallelized, and the limits of computational resources are of course met earlier than with the parallelized code. Since stair-casing is used, the convergence can be guaranteed only with a relatively long bunch (allowing more cells over the bunch length), as the tapered sections slow down the convergence of the results with decreasing cell size. Numerical results in the case when only

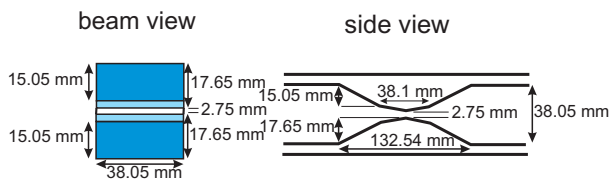

Figure 6: The ILC collimator geometry.

the direct integration is taken into account are shown in Fig. 7 (a). The results with the proposed scheme agree well with the results of PBCI-code [11]. When the indirect wake potential calculation is taken into account, we obtain the result in Fig. 7 (b). The indirect integration scheme was not available in the version of PBCI used for these simulations.

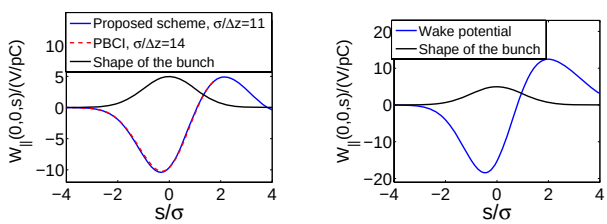

(a) (b)

Figure 7: (a) The longitudinal wake potential without indirect integration. A comparison with PBCI. (b) The longitudinal wake potential with the indirect integration included.

Finally we compare the 2D scheme with ECHO [2]. At the

[1] The bunch length in the actual experiments was 300 μm.

[2] ECHO is a wake field code based on the implicit scheme [5].

same time we demonstrate the convergence of the results with decreasing cell size. The test structure is shown in Fig. 8. We simulate the collimator with stair-cased geometry approximation. Conformal techniques are available but stair-cased comparison allows to better see the differences in accuracy between the methods. We calculated

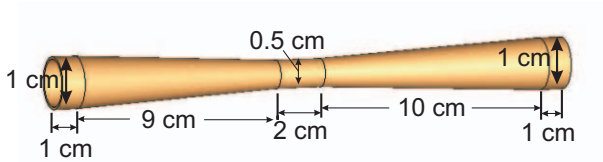

Figure 8: A gently tapered circular cylindrically symmetric collimator.

the longitudinal wake potential using four different mesh resolutions: $\sigma/\Delta z = 5$, $\sigma/\Delta z = 10$, $\sigma/\Delta z = 20$ and $\sigma/\Delta z = 40$. The bunch length is $500\ \mu m$. The convergence of the results with decreasing cell sizes can be observed in Figs. 9 (a) and 9 (b). It may be noticed that the accuracy with the proposed scheme is similar to ECHO with about two times coarser mesh.

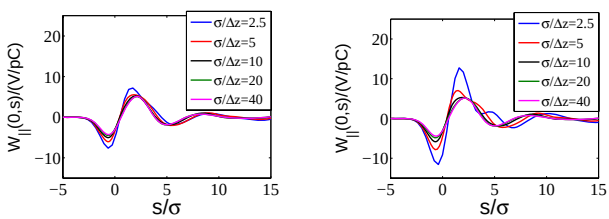

Figure 9: (a) Longitudinal wake potential with the proposed explicit scheme. Stair-cased geometry representation. (b)Longitudinal wake potential with the implicit scheme of [5] (computer code ECHO). Stair-cased geometry representation.

About $20 - 40$ cells per σ are required to guarantee good accuracy of the results for the collimator in Fig. 8. Calculations using conformal versions of the 2D codes show that only 5 cells per σ are enough to achieve similar accuracy. In 3D, the sufficient computation time is roughly inversely proportional to the fourth power of the cell size. Obviously, computational saving in large 3D problems would be huge if conformal scheme could be used. The present 3D implementation is based on stair-casing, but conformal extensions are an important topic of future work.

CONCLUSIONS

Low-dispersion FDTD schemes for time-domain wake field simulations in accelerator structures have been presented and validated. The proposed explicit schemes are free of numerical dispersion in main coordinate axis directions and can be used with the moving window in large accelerator simulations.

REFERENCES

[1] I. Zagorodnov, T. Weiland, *TE/TM scheme for computation of electromagnetic fields in accelerators*, J. Comp. Phys. 207, (2005), 69–91.

[2] I. Zagorodnov, T. Weiland, *TE/TM field solver for particle beam simulations without numerical Cherenkov radiation*, Phys. Rev. ST-AB **8**, 042001 (2005).

[3] T. Lau, E. Gjonaj, T. Weiland, *Particle-in-cell based beam dynamics simulations*, Proc. of EPAC 2004, Lucerne, Switzerland, pp. 170–172.

[4] A. Novokhatski, M. Timm, T. Weiland, *Transition dynamics of the wake fields of ultra short bunches*, in Proc. of the ICAP 1998, vol. 132, Monterey, California, USA, 1998.

[5] I. Zagorodnov, R. Schuhmann, T. Weiland, *Long-time numerical computation of electromagnetic fields in the vicinity of a relativistic source*, J. Comp. Phys. 191, (2003) 525–541.

[6] K. S. Yee, *Numerical solution of initial boundary value problems involving Maxwell's equations in isotropic media*, IEEE Trans. Antennas Propag., Vol. 14, No. 3, 1966, pp. 302–307.

[7] T. Weiland, *A discretization method for the solution of Maxwell's equations for six-component fields*, International Journal of Electronics and Communication (AEÜ), Vol. 31 (1977), pp. 116–120.

[8] G. Strang, *On construction and comparison of difference schemes*, SIAM J. Numer. Alal., Vol 5, 1968, pp. 506–516.

[9] J. B. Cole, *A high-accuracy realization of the Yee algorithm using non-standard finite differences*, IEEE Trans. Microw. Theory Tech., vol. 45, no. 6, June 1997, pp. 991–996.

[10] J. B. Cole, *A high-accuracy Yee algorithm based on non-standard finite differences: new developments and verifications*, IEEE Trans. Antennas Prop., vol. 50, no. 9, Sept 2002, pp. 1185–1191.

[11] W.F.O. Müller, X. Dong, E. Gjonaj, R. Hampel, M. Kärkkäinen, T. Lau, T. Weiland, *Massively parallel wake field computations in long accelerator structures*, in Proc. LINAC 2006, USA.

[12] T. Weiland, *On the numerical solution of Maxwell's equations and applications in accelerator Physics* , Particle Accelerators, Vol. 15 (1984), pp. 245–292.

[13] T. Weiland, *Comment on wake field computation in time domain*, Nuclear Instruments and Methods (NIM), Vol. 216 (1983), pp. 31–34.

[14] T. Weiland, *Transverse Beam Cavity Interaction, Part I: Short Range Forces*, Nuclear Instruments and Methods (NIM), Vol. 212 (1983), pp. 13–34.

[15] K. Bane, T. Weiland, *Wake force computation in the time domain for Long Structures*, Proceedings of the 12th International Conference on High Energy Accelerators, Chicago, 1983, pp. 314–316.

[16] H. Henke, W. Bruns, *Calculation of wake potentials in general 3D structures*, proc. EPAC 2006.

[17] I. Zagorodnov, *Indirect methods for wake potential integration*, submitted to Phys. Rev. ST-AB, 2006.